Received: 22 July 2024 | Revised: 2 October 2024 | Accepted: 10 November 2024

DOI: 10.1111/jace.20290

Journal of the American Ceramic Society

RESEARCH ARTICLE

3D-printed porous mullite lattice structures by hybrid direct ink writing of silicone suspension-emulsions

Valeria Diamanti | **Hamada Elsayed** | **Enrico Bernardo**

Department of Industrial Engineering, Università degli Studi di Padova, Padova, Italy

Correspondence
Enrico Bernardo, Department of Industrial Engineering, Università degli Studi di Padova, 35131 Padova, Italy.
Email: enrico.bernardo@unipd.it

Abstract

Silicones added with nano-sized alumina particles are already known as starting materials for phase pure mullite ceramics, synthesized at quite low temperatures. The present paper deals with a fundamental upgrade, based on a novel suspension-emulsion concept, for the easy fabrication of highly porous lattice structures. An aqueous suspension of γ-Al_2O_3 nanoparticles in water was first distributed as emulsion within an "oily phase," consisting of a silicone/acrylates blend, with the help of a surfactant. The mixture was later employed to fabricate highly porous structures (~80% open porosity), by direct ink writing, that is, an extrusion-based 3D printing technology requiring specific rheological behavior of the feedstock ink. Finally, the structures were rapidly stabilized through a photo-polymerization step (configuring a form of "hybrid" direct ink writing). The presence of water also allowed the application of a freeze-curing procedure, for a second series of samples. The abundant water vapor release from the starting mixtures, upon firing (up to 1300°C), led to structures with enhanced pore interconnectivity. The freeze-curing protocol proved beneficial to the homogeneity of pore distribution and to the achievement of high strength-to-density ratios.

KEYWORDS
mullite, polymer precursor, printing

1 | INTRODUCTION

Mullite ($3Al_2O_3 \cdot 2SiO_2$) is a refractory alumino-silicate that has earned significant interest for several applications, from aerospace components to biomedical implants.[1] This ceramic, in fact, shows excellent physical and chemical properties, such as low density, low electrical and thermal conductivities, low thermal expansion, high chemical and thermal stability, as well as creep resistance.[2] In particular, mullite in the form of porous structures with suitable mechanical integrity appears as highly suitable for filters and catalyst supports.[3] Recent studies comprise the fabrication of support structure for modern metal–organic frameworks (MOFs), for applications in catalysis, sensing, and adsorption.[4]

The microstructure and properties of mullite ceramics strongly depend on the adopted synthesis route and the corresponding sintering temperatures. Well-established

methods to obtain mullite, starting from conventional raw materials, such as clays and alumina, generally require high processing temperatures.[2] Therefore, extensive research has been conducted over the years to yield phase pure mullite at lower temperatures. Sol–gel process, as an example, has been reported to induce complete mullitization between 1000°C and 1350°C, due to the high purity and distribution of the precursors at a quasi-atomic scale.[5]

Silicone polymers, filled with nano-sized alumina particles, have been investigated as possible alternative raw materials, always in the perspective of lower processing temperatures, for nearly 20 years.[6–8] The approach relies mainly on the high reactivity of both γ-Al_2O_3 nanoparticles ("active" fillers) and amorphous silica resulting from the thermo-oxidative decomposition of the polymers.

The use of silicones actually has advantages well beyond low processing temperatures and phase purity. In fact, silicones belong to the vast range of preceramic polymers, that is, materials that can be first shaped at nearly room temperature, like conventional polymers, and then transformed into ceramics by heat treatment.[9] Among plastic-forming technologies, additive manufacturing (AM) technologies are receiving an increasing interest. When applied to preceramic polymers, AM technologies allow for the fabrication of a variety of porous ceramic components, with particularly complex shapes.[10,11] In the case of mullite, interesting results were obtained by digital light processing (DLP) applied to photocurable blends of silicone polymers, combined with γ-Al_2O_3.[8]

The present paper is dedicated to the application of another AM technology to the manufacturing of highly porous mullite ceramics. More precisely, the investigation concerned Direct Ink Writing (DIW) of silicone-based pastes ("inks"), in which the control of rheology was realized by means of an unprecedented methodology.

DIW, originally patented as "Robocasting" by Cesarano,[12] is an extrusion-based additive manufacturing technology, which employs a layer-by-layer robotic deposition of the ink to fabricate 3D structures with complex architectures.[13] It typically requires inks with a shear thinning behavior, according to which the viscosity of the paste decreases with increasing shear rate, enabling easy ejection upon extrusion from the deposition nozzle. A fast recovery of the viscosity, once out from the nozzle, however, is also necessary to retain the as-printed shape and minimize the deformations.[11,14]

For many particle-based formulations, the rheological requirements are hardly fulfilled. In fact, the powder dimension typically controls the type of nozzle that can be effectively employed to extrude the ink. This, in turn, affect some common issues such as surface quality, minimum feature dimensions achievable, nozzle clogging, ink drying, etc.[15] Although nano-sized particles may seem favorable, the potential to enhance printing resolution and avoid nozzle clogging is compromised by substantial increases in viscosity.[16]

The drawbacks associated with solid fillers may be avoided when operating with emulsions.[17,18] Mixtures of enhanced homogeneity were easily achieved just by dispersing active fillers in form of liquid nano-droplets, deriving from salt with low melting point (e.g., hydrated calcium nitrate, acting as CaO precursors), within matrices of photocurable liquid silicone/acrylate blends. The nano-droplets do not coalesce, according to the use of surfactants, and simply transform into nanoparticles within cured matrix, later subjected to ceramization. The quasi-molecular mixing of the active filler enables the obtainment of glass matrix composites.[17]

The investigation here presented recovered the concept of emulsions, but the dispersed phase did not correspond to any molten salt but rather to γ-Al_2O_3 nanoparticles suspended in deionized water.

A silicone/acrylates blend was later added with this aqueous suspension of γ-Al_2O_3 nanoparticles, configuring a suspension-emulsion ink, with suitable pseudoplastic behavior for DIW. The introduction of acrylates offered the possibility to stabilize printed lattice structures beyond viscosity recovery, by photopolymerization. The homogeneity of the dispersion of the active filler yielded again mullite at relatively low firing temperatures.

Water actually played a multiform role. Besides acting as dispersant for Al_2O_3 nanoparticles, it was expected to enhance the gas evolution upon firing, to obtain highly porous structures. Quite surprisingly, it provided also an additional opportunity for the mixing of the constituents, after printing, according to the freezing of the aqueous suspension.

2 | EXPERIMENTAL PROCEDURE

2.1 | Preparation of emulsions and DIW-printing

The whole preparation process is illustrated by Figure 1. As noticeable, the same procedure was employed to produce and print the mixtures in the form of 3D structures which later followed two different postprocessing routes.

In analogy with the first investigations on polymer-derived mullite, γ-Al_2O_3 nano-sized powders were used as alumina source.[6] H44 silicone (Silres® H44, Wacker-Chemie GmbH, Munich, Germany) was considered as silica source, according to a H44/γ-Al_2O_3 weight ratio of 0.62. The ceramic yield of H44 was assumed as 53%, according to previous studies concerning thermo-oxidative treatments.[19]

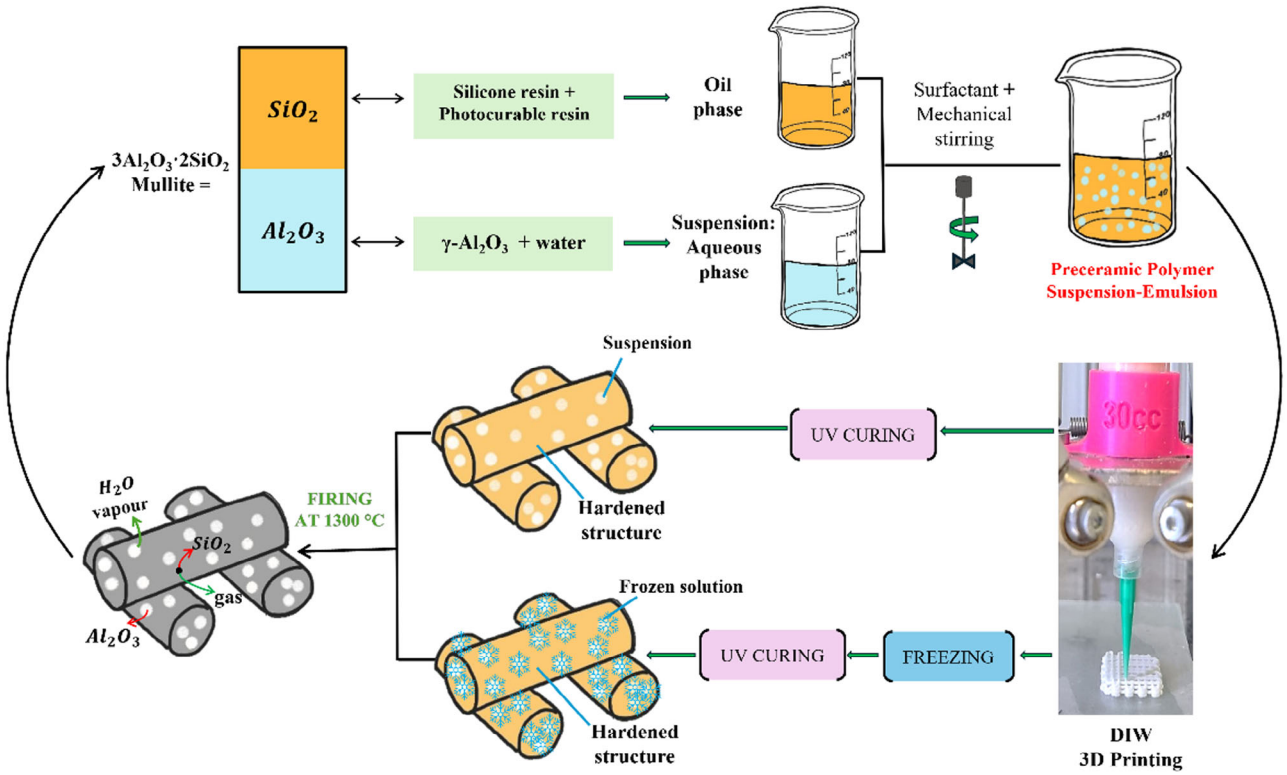

FIGURE 1 Scheme of the overall processing method employed for both normal and frozen samples.

TABLE 1 Ceramic yields by component.

Component	Amount in batch (g)	Oxide yield (g)
Silres H44	2.48	$2.48 \times 0.53 = 1.31$ (SiO_2)
Standard blend (FunToDo)	3	Complete burn-out
Surfactant Span80	1.75	Complete burn-out
γ-Al_2O_3 nanoparticles	3.98	$3.98 \times 1 = 3.98$ (Al_2O_3)
Boric anhydride (B_2O_3)—*used in selected formulations*	0.12	0.12
Water	12	Complete evaporation

Table 1 reports the proportions for typical batches. Emulsions were prepared starting from an oily phase, in turn obtained by dissolving H44 (solid powder) in commercial (liquid) photocurable acrylic resin (Standard Blend Transparent, FunToDo, Alkmaar, The Netherlands). The mixture was subsequently added with Span 80 (Sorbitan Monooleate, TCI-Tokyo Chemical Industry, Tokyo, Japan), a nonionic surfactant and subjected to mechanically mixing for 5 min at 300 rpm (AM 20-D ARGOlab, Carpi MO—Italy), before being left overnight.

The "aqueous" phase corresponded to a suspension of γ-Al_2O_3 nanoparticles. The particles were gradually cast in deionized water, under magnetic stirring; the suspension was later sonicated for 15 min in order to obtain a homogeneous dispersion. Selected batches comprised also boric anhydride (granulated, ≥98%, Sigma-Aldrich, Merck KGaA spa, Darmstadt, Germany), added to the aqueous phase before sonication; the amount of additive was calculated in order to represent a ≈2 wt.% addition to the overall ceramic mass (sum of silica, from H44, and alumina filler), following the literature of sintering aids of mullite.[20,21]

"Oily" and "aqueous" phases were finally homogenized. Aqueous suspensions were cast in H44/acrylates blends under intensive mechanical stirring (2200 rpm), for 10 min; the resulting emulsions were transferred in 30 cm^3 plastic syringes and subjected to a de-foaming process (2200 rpm for 1 min) by means of a conditioning mixer (THINKY ARE-250, planetary centrifugal mixer) in order to produce fully bubble-free feedstock.

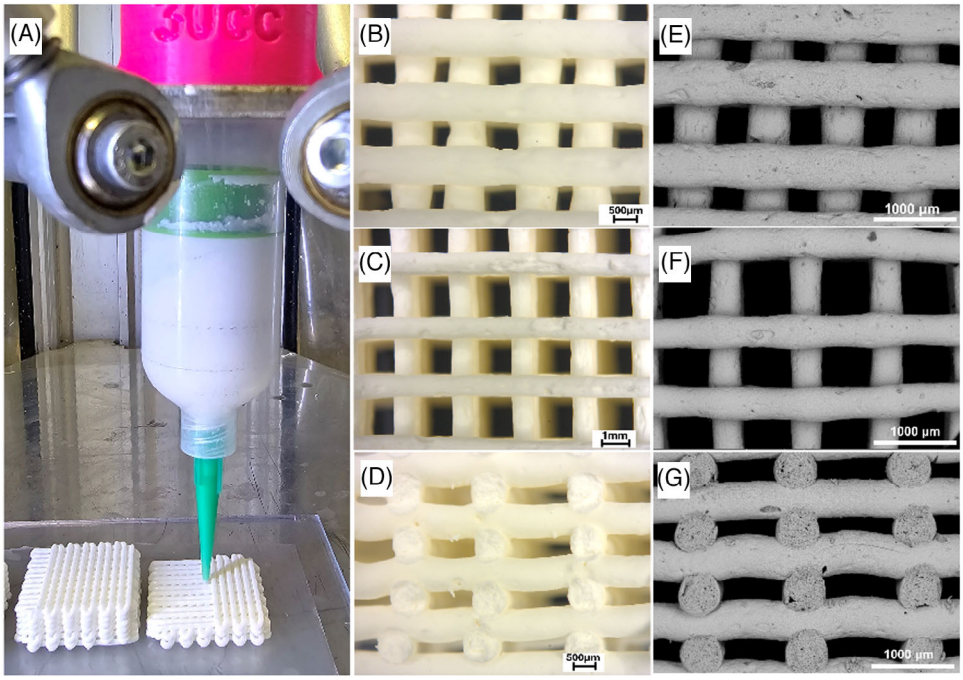

FIGURE 2 (A) Detail of the printing head; green bodies (B) type 8 top view, (C) type 16 top view, (D) type 16 side view; fired samples (E) type 8 top view, (F) type 16 top view, (G) type 16 side view.

Syringes were finally mounted in a 3-axis DIW printer (Delta WASP 2040 PRO Wasp s.r.l., Italy), which allowed the printing of the geometries by a layer-by-layer extrusion of the ink, on a PTFE substrate, at room temperature (Figure 2A). The amounts of components employed allowed the printing of several specimens (approximately 7–8 for batch). In particular, by using 0.84 mm conical nozzle two different geometries were fabricated: 800–800 scaffolds (type 8) with a line spacing equal to the filament size (Figure 2B) and 800–1600 scaffolds (type 16) with a line spacing two times the filament size (Figure 2C).

Once printed, the specimens were split into two groups according to different subsequent procedures applied. Samples N, just after the printing, were simply exposed to a UV-lamp (Prusa CW1, Prague, Czech Republic, operating at $\lambda = 405$ nm), for 40 min, to activate the polymerization of the photocurable resin. Samples F, instead, were placed in a refrigerator at −18°C, for 4 h, before applying the curing step in the UV-lamp.

Finally, samples in both group N and group F underwent the polymer-to-ceramic conversion ("ceramization") by a two-step heat treatment in flowing air (Elite thermal systems limited, Tersid srl, Italy): 0.5°C/min up to 500°C, dwell of 3 h followed by another ramp of heating at 5°C/min up to 1300°C and dwell of 2 h. The sintering temperature of 1300°C was chosen as the optimal one after several trials according to previous studies.[6,22]

2.2 | Characterization

Characterizations were conducted at every stage of the processing. Before printing, rheology experiments were conducted to determine whether the ink possessed appropriate rheological properties for extrusion; in particular, the recovery time had to be precisely assessed, to understand the shape retention and self-supporting capability for the structures.[14,23,24] The measurements were performed in isothermal conditions at 25°C employing a rotational rheometer (MCR302, Anton Paar GmbH, Graz, Austria), equipped with a 40 mm cone-and-plate geometry and a fixed distance between the two plates of 0.33 mm. Two types of tests were performed:

1. flow curves with shear rate ranging from 0.1 to 100 s^{-1}, to derive the viscosity and the shear stress trends as function of the shear rate;
2. thixotropy tests, to evaluate the recovery of viscosity, divided into three steps (30 s at a shear rate of 0.003 s^{-1} to simulate the rest state of the ink before printing; 30 s at 0.006 s^{-1} to exceed the flow point and thus simulate the extrusion process; 30 s at 0.003s^{-1} to mimic the rest state of the filament after deposition).

Morphological and microstructural observations, before and after heat treatment, were performed by optical stereomicroscopy (AxioCam ERc 5s Microscope Camera, Stemi

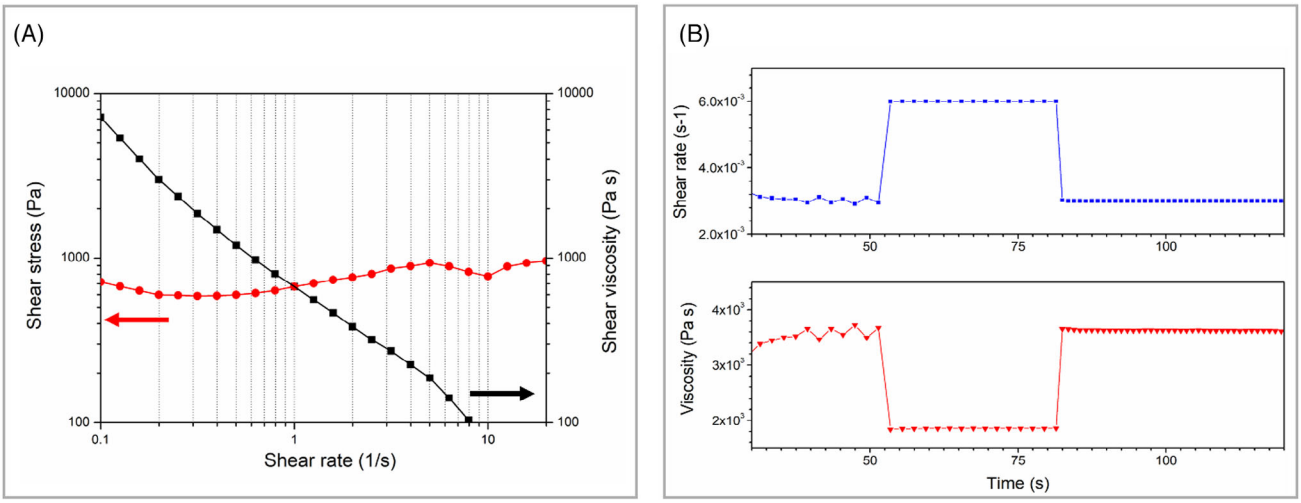

FIGURE 3 (A) Shear stress and viscosity versus shear rate; (B) viscosity recovery test.

2000-C, Zeiss, Jena, Germany) and scanning electron microscopy (FEI® Quanta 200 ESEM, Eindhoven, The Netherlands).

Density and porosity values, on green and fired samples, were determined measuring the geometrical (bulk) density as mass/volume ratio by means of an analytical balance and a digital caliper, respectively, and the apparent density by means of the He-gas pycnometer (Ultrapyc 3000, Anton Paar Srl, Rivoli, Italy). Furthermore, the linear and volumetric shrinkage due to the polymer-to-ceramic conversion were determined.

Ceramized samples underwent mineralogical analysis through X-Ray diffraction (Bruker D8 Advance, Karlsruhe, Germany), conducted in the 2θ range of 10–70°, with a step size of 0.05° and a counting time of 1 s.

The compressive strength of fired samples was determined by means of a universal material testing machine (Quasar 25, Galdabini S.p.A., Cardano al Campo, Italy). The tests were performed at a crosshead speed of 0.5 mm/min. The final results were averaged from tests conducted on at least five samples.

3 | RESULTS AND DISCUSSION

The developed suspension-emulsion ink, as shown by Figure 3A, exhibited a typical shear-thinning behavior, with decreasing viscosity with increasing shear rate, useful to realize an easy flow through the deposition nozzle.[24] It can be noted that the shear stress slightly increased with increasing shear rate, up to 1 kPa, at a shear rate of 5 s^{-1}, which can be assumed as yield value σ_y; the decrease of stress, with increase of shear rate up to 10 s^{-1}, can be seen as a transition from a solid-like to a liquid-like behavior. Moderate pressures were found to allow for proper fluidity.

The transition was reversible. As shown by Figure 3B, changes in shear rate, from 0.003 to 0.006 s^{-1} were accompanied by simultaneous changes in viscosity. It can be concluded that the rheological behavior was in favor of both easiness of ejection from deposition nozzle and ability to preserve the shape. The latter is illustrated by the absence of filament sagging in Figure 2D and G.

The particular formulation enabled further shape stabilization. In fact, the curing step in the UV chamber prevented any risk of viscous collapse over time. Cured samples could be easily handled, when moved to the ceramization furnace, without any deformation. The stiffness, resulting from UV curing, was appreciated for samples of both N and F groups (the latter, before curing, underwent a freezing step).

A key to success, for various mullite-yielding formulations, is the development of a phase-pure ceramic. The presence of several additives generally complicates the understanding of the real ceramic yield of preceramic polymers.[25] The adopted balance between alumina and polymer-derived silica actually deviates from that of stoichiometric mullite ($3Al_2O_3{\cdot}2SiO_2$), with a slight Al_2O_3 excess, in agreement with the literature,[26] set to limit the separation of SiO_2 as cristobalite. Figure 4A evidences the presence of some cristobalite (alpha phase, PDF#77-1317) attributable to the formation, as main phase, of Al-richer mullite solid solution, upon firing at 1300°C. The flat background suggests a high degree of crystallinity. The contamination was easily removed; the introduction of B_2O_3 enhanced the ionic interdiffusion, by providing some liquid phase upon firing,[27] and realized nearly phase pure mullite. The solubility of B_2O_3 in water[28] likely promoted a homogeneous distribution of the additive.

The additive was effective in supporting the already significant reactivity of the main constituents. Figure 4B

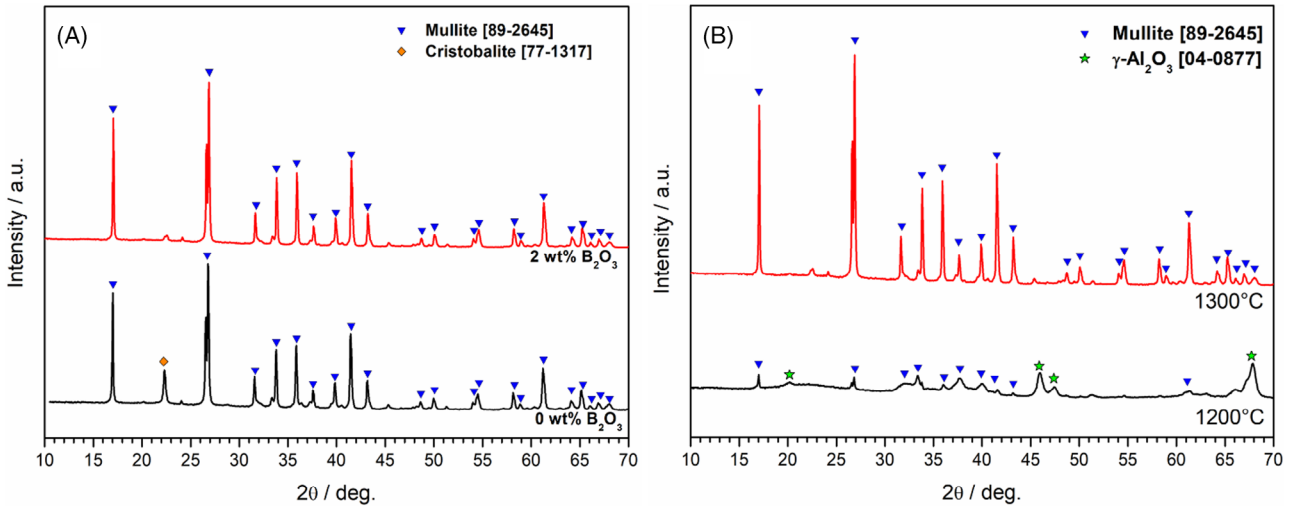

FIGURE 4 XRD patterns: comparison between (A) formulations with (red line) and without (black line) sintering aids at 1300°C and (B) firing temperatures of 1200°C (black line) and 1300°C (red line).

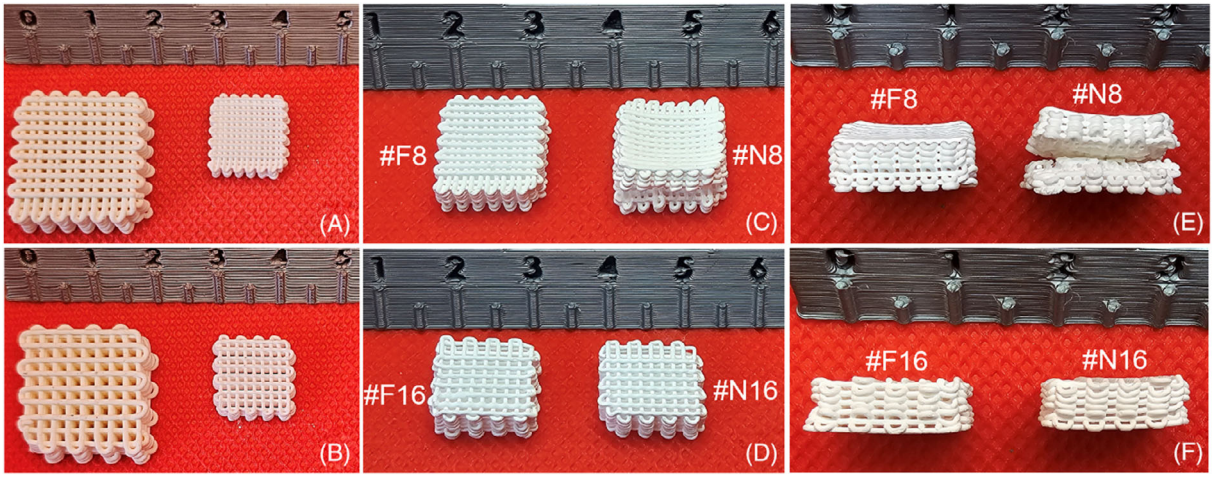

FIGURE 5 Comparison between before (left) and after (right) firing: (A) type 8, (B) type 16; comparison between frozen (left) and normal (right) samples: (C) type 8, (D) type 16; side view comparison between frozen (left) and normal (right) samples: (E) type 8, (F) type 16.

shows that some mullite formed even at 1200°C, which is below the recognized limit for diphasic systems to yield mullite (1250°C). [22]

The formulation here presented is evidently just an example. Multiple combinations of silicone/alumina ratio, B_2O_3 amount, firing temperature etc. can be envisaged, but they are beyond the scope of this paper.

Figure 5A and B show the samples in green (on the left) and fired (on the right) states. The marked shrinkage (linear shrinkage ≈60%; volumetric shrinkage ≈75%) is mainly attributed to the gaseous by-products released during the decomposition of reagents and to vapor release from water removal. Nonetheless, despite the remarkable change in volume, the regular structure and ordered porosity given by the adopted printing model was retained for all the samples after the ceramic conversion.

Additionally, scanning electron microscopy (Figure 2E and F) revealed the absence of both surface cracks and chemical gradients after sintering. These features were observed for all samples, regardless of the protocol they were subjected to after printing.

A major drawback, in the firing of samples of the #N8 group, was the repeated macrocracking of lattices. As shown by Figure 5C and E, most of #N8 samples underwent splitting in two separate blocks and distortion, which was not observed in other samples. This defect was likely due to development of some stresses, during ceramic conversion, between external parts (undergoing faster heating) and internal parts; these stresses reasonably caused delamination according to the poor interpenetration of the filaments in the contact region.

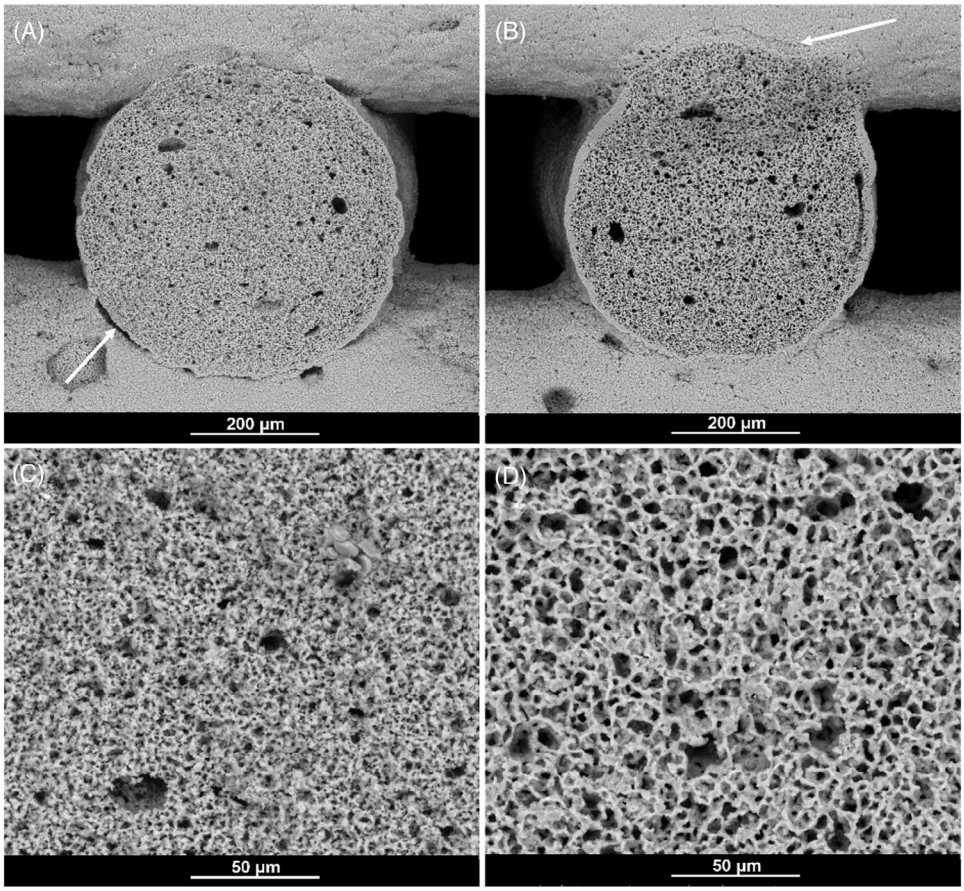

FIGURE 6 SEM images of the strut cross-section: (A) #N8, (B) #F8; higher magnifications of the strut cross-section: (C) #N8, (D) #F8.

The freezing step, applied before UV-induced consolidation, proved to be effective in preventing any defects, even for samples with the same spacing of filaments (#F8). According to the authors, this was attributed to a "micro-mixing" effect observed in the microstructure of the samples subjected to freezing. Specifically, before UV irradiation, the as-printed samples were still viscous pastes. The volumetric expansion of water upon freezing could force the viscous material inside the filaments to move and reorganize. The subsequent curing step, under UV, enabled the consolidation of the new structure, especially at the junction points of the filaments. As a result, layer cohesion improved, ultimately leading to enhanced structural integrity and, thus, to defect-free structures after the ceramic conversion.

As an example, the arrow in Figure 6A highlights incomplete welding of overlapped filaments, in "cured just after extrusion" samples; on the contrary, overlapped filaments, for samples undergoing an intermediate freezing step, present "mixing zones" (see arrow in Figure 6B). The situation is unprecedented (to the authors' knowledge analogies can be found only in some freeze-casting experiments, when frozen solvent temporarily acts as binder, by holding the structure together)[29] and evidently deserves future efforts to fully realize the potential (acting on both freezing temperatures and cooling rates), but undoubtedly substantiates the high flexibility of the proposed suspension-emulsion approach.

Figure 6 actually allows for further observations, specifically on pore distribution. UV curing evidently affected the free surfaces of the reticulated structures which were more exposed to UV rays. Therefore, as shown by Figure 6A and B, upon curing, the exposed surface became more rigid and created a denser outer layer around the filaments. In these exposed layers the cross-linking prevented the extensive formation of bubbles, according to water evaporation and silicone transformation (H44 is known to exhibit some foaming),[30] at the early stages of firing, well visible in the filament cores (Figure 6C). The freezing step led to larger pores, but more homogeneously distributed (Figure 6D). In other words, water emerges as multiform component: as "nano-particle carrier" it led to the observed easy extrusion, *during* printing; *after* printing, it acted as a porogen, for uncured material, with additional microstructural control realized by freezing. Again, the present paper can provide only some examples of possible combinations of processing parameters contributing to the microstructure (e.g., amount of water and curing depth,

TABLE 2 Results from density and compressive strength determinations.

Scaffold type	Geometric density ρ_g (g/cm^3)	Apparent density ρ_a (g/cm^3)	True density ρ_t (g/cm^3)	Open porosity OP (vol%)	Total porosity TP (vol%)	Compressive strength σ_c (MPa)
#N8	0.63 ± 0.03	2.98 ± 0.03	3.02 ± 0.01	78 ± 1	79 ± 1	4.6 ± 1.3
#N16	0.55 ± 0.04	3.04 ± 0.01	3.05 ± 0.01	81 ± 1	82 ± 1	5.1 ± 0.9
#F8	0.68 ± 0.05	3.03 ± 0.02	3.03 ± 0.01	76 ± 1	78 ± 2	8.2 ± 2.3
#F16	0.56 ± 0.1	3.05 ± 0.02	3.05 ± 0.01	81 ± 3	82 ± 3	7.5 ± 2.1

in turn conditioned by the lighting and by the presence of photo-absorbers, and in turn defining the amount of "soft" material, in the struts, subjected to bubble formation), to be explored in the future.

Table 2 reports porosity and density values for the developed lattice structures. The apparent density, measured through He-gas pycnometer, yielded values of 3–3.1 g/cm^3, which are very close to the theoretical density of mullite ceramics (3.16 g/cm^3).[8] This finding supports the assumption of nearly completely open porosity. The densified layers, in other words, despite having fewer pores, allowed for some gas flow; that is, they did not compromise the pore interconnectivity. Another proof is the fact that the porosity values (76–82%) well exceeded the calculated "theoretical geometrical porosity," resulting from the overlapping of dense, homogeneous cylindrical filaments (≈60% for #N8 and #F8, ≈73% for #N16 and #F16). In our opinion, the high levels of porosity, coupled with the excellent thermal stability of mullite, are promising in the perspective of application of the printed lattices as catalyst supports, where precise control over pore size and distribution is crucial.[3]

The compressive strength values, also shown in Table 2, varied between 4.6 and 8.2 MPa. It can be noted that samples of the F group exhibited higher mechanical strength than samples of the N group, confirming the enhanced homogeneity and cohesion between filaments promoted by the freezing procedure. In fact, with overall porosity practically unchanged, for a certain spacing of filaments, the improved homogeneity, with freezing, evidently enhanced the strength. Furthermore, as expected, in group F the geometry with a higher number of overlapping filaments and thus, less open porosity (#F8), exhibited higher compressive strength values. Nonetheless, the same behavior was not observed in group N, where we would expect the compressive strength values for #N8 to exceed those of #N16, which did not happen. Once again, we explained this behavior as a consequence of the delamination phenomena observed in #N8 samples, which led to defective and less resistant structures.

In general, any evaluation of the strength of cellular ceramics cannot be made without considering the scaling of strength operated by the same porosity. An undoubted reference, in this field, is the Gibson and Ashby model for open-celled "bending dominated" structures (i.e., networks of interconnected beams),[31] which predicts the compressive strength (σ_c) as a function of the bending strength of the solid phase (σ_{bend}) and relative density (ρ_{rel}), as follows:

$$\sigma_c = C \cdot \sigma_{bend} \cdot \rho_{rel}^{3/2}.$$

ρ_{rel} is inferred from the total porosity P ($\rho_{rel} = 1 - P/100$); C is a dimensionless constant (≈0.2). The equation is interesting also for an indirect use. Introducing the experimental data of compressive strength and relative density, we could infer, to fit the data, values of "apparent" strength of the solid phase σ_{bend}. These values, for samples of the F group, varied from ≈350 MPa (#F8) to ≈450 MPa (#F16), well exceeding the analogous values for samples of the N group (from ≈220 MPa for #N8 to ≈300 MPa for #N16). The practical identity of apparent (i.e. estimated) σ_{bend} values, for F samples, with the real bending strength of mullite ceramics, assessed by testing dense bars,[32] is reputed as an evidence of bodies with optimized strength-to-density.

4 | CONCLUSIONS

Highly porous mullite lattice structures were successfully fabricated by Direct Ink Writing 3D printing of emulsions based on a silicone polymer. More precisely, the investigation defined novel "suspensions-emulsions," in which water acted as a dispersant for γ-Al_2O_3 nanoparticles. The approach recovered the high reactivity of silicone/γ-Al_2O_3 nanoparticles, discovered nearly two decades ago, but not exploited so far in DIW 3D printing. The high reactivity is the key reason for the nearly complete mullitization by firing in air at only 1300°C.

Water played a multiform role in "suspensions-emulsions." Silicone-based pastes, despite the substantial content of alumina filler (the Al_2O_3/SiO_2 weight ratio in mullite is quite high), had suitable rheological properties to be extruded and shaped by DIW. The contribution of water, during printing, however, was far less remarkable than that after printing. A truly "hierarchical porosity," that is, a distribution of pores on different scale, was easily realized, since macropores from the stacking of

extruded filaments could be accompanied by gas bubbles determined by water evaporation.

All the structures exhibited high volumetric shrinkage (≈75%) and crack-free surfaces after the ceramic conversion. In addition, the freezing protocol proved to be particularly beneficial to the homogeneity of the microstructure. The discovered "micro-mixing" of silicone pastes indeed prevented macroscopic defectivity (such as delamination of poorly interconnected overlapped filaments) as well as favored the achievement of remarkable strength-to-density ratios. Frozen samples, in fact, exhibited compressive strength data consistent with a solid phase having excellent bending strength (350–450), in good agreement with data reported for mullite dense bars (≈330 MPa).

The adopted approach is highly flexible, starting from the inclusion of photocurable acrylates, set to achieve a fast stabilization of extruded structures. UV curing actually had some interplay with the pore evolution, with water evaporation, still to be explored. In general, the processing conditions, as well as the proportions between constituents, may configure a huge number of combinations, to be investigated in the future for a new generation of porous mullite ceramics.

ACKNOWLEDGMENTS

The authors thank Dr Federico Zorzi (University of Padova) for experimental assistance in scanning electron microscopy.

Open access publishing facilitated by Universita degli Studi di Padova, as part of the Wiley - CRUI-CARE agreement.

ORCID

Valeria Diamanti https://orcid.org/0009-0005-7664-2426

Hamada Elsayed https://orcid.org/0000-0002-9818-4498

Enrico Bernardo https://orcid.org/0000-0003-4934-4405

REFERENCES

1. Viswanath B, Darshankumar J, Gunapriya B, Karthi M, Sankaramoorthy T, Murugesan K. Preparation and characterization of mullite ceramic nano powder for use in nanocomposites. *AIP Conf Proc*. 2022;2446:120001. https://doi.org/10.1063/5.0108979
2. Roy R, Das D, Rout PK. A review of advanced mullite ceramics. Eng Sci. 2022;18:20–30. https://doi.org/10.30919/es8d582
3. Schneider H, Komarneni S, Okada K. Mullite synthesis. In: Schneider H, Komarneni S, editors. Mullite: WILEY-VCH Verlag GmbH & Co. KGaA, 2005. p. 251–85.
4. Hou Z, Tian Z, Zhao J, Liu L, Zhang W, Huang Z, et al. In situ growth of ZIF-8 on mullite whiskers to form millimeter-sized composite beads for water treatment. Sep Purif Technol. 2024;329:125170. https://doi.org/10.1016/j.seppur.2023.125170
5. Cividanes LS, Campos TMB, Rodrigues LA, Brunelli DD, Thim GP. Review of mullite synthesis routes by sol–gel method. J Sol-Gel Sci Technol. 2010;55(1):111–25. https://doi.org/10.1007/s10971-010-2222-9
6. Bernardo E, Colombo P, Pippel E, Woltersdorf J. Novel mullite synthesis based on alumina nanoparticles and a preceramic polymer. J Am Ceram Soc. 2006;89(5):1577–83. https://doi.org/10.1111/j.1551-2916.2006.00963.x
7. Gorjan L, Tonello R, Sebastian T, Colombo P, Clemens F. Fused deposition modeling of mullite structures from a preceramic polymer and γ-alumina. J Eur Ceram Soc. 2019;39(7):2463–71. https://doi.org/10.1016/j.jeurceramsoc.2019.02.032
8. Schmidt J, Altun AA, Schwentenwein M, Colombo P. Complex mullite structures fabricated via digital light processing of a preceramic polysiloxane with active alumina fillers. J Eur Ceram Soc. 2019;39(4):1336–43. https://doi.org/10.1016/j.jeurceramsoc.2018.11.038
9. Colombo P, Mera G, Riedel R, Sorarù GD. Polymer-derived ceramics: 40 years of research and innovation in advanced ceramics. J Am Ceram Soc. 2010;93(7):1805–37. https://doi.org/10.1111/j.1551-2916.2010.03876.x
10. Chaudhary RP, Parameswaran C, Idrees M, Rasaki SA, Liu C, Chen Z, et al. Additive manufacturing of polymer-derived ceramics: materials, technologies, properties and potential applications. Prog. Mater. Sci. 2022;128:100969. https://doi.org/10.1016/j.pmatsci.2022.100969
11. Colombo P, Schmidt J, Franchin G, Zocca A, Günster, J. Additive manufacturing techniques for fabricating complex ceramic components from preceramic polymers. Am Ceram Soc Bull. 2017;96:16–23
12. Cesarano III J., Calvert PD. Freeforming objects with low-binder slurry. U.S. Patent No 6,027,326. 2000
13. Saadi MASR., Maguire A., Pottackal NT., Thakur MSH., Ikram M.M, Hart AJ., et al. Direct ink writing: a 3d printing technology for diverse materials. Adv Mater. 2022;34, 2108855. https://doi.org/10.1002/adma.202108855
14. Wei P, Cipriani C, Hsieh C-M, Kamani K, Rogers S, Pentzer E. Go with the flow: rheological requirements for direct ink write printability. J Appl Phys. 2023;134(10):100701. https://doi.org/10.1063/5.0155896
15. Franchin G, Elsayed H, Botti R, Huang K, Schmidt J, Giometti G, et al. Additive Manufacturing of Ceramics from Liquid Feedstocks. Chin J Mech Eng Addit Manuf Front. 2022;1(1):100012. https://doi.org/10.1016/j.cjmeam.2022.100012
16. Hanemann T. Influence of particle properties on the viscosity of polymer–alumina composites. Ceram Int. 2008;342:099–2105. https://doi.org/10.1016/j.ceramint.2007.08.007
17. Stabile FM, Famengo A, Pedron D, Elsayed H, Bernardo E. Functional bioglass/carbon nanocomposite scaffolds from vat photopolymerization of a novel preceramic polymer-based nanoemulsion. Addit. Manuf. 2023;75:103731. https://doi.org/10.1016/j.addma.2023.103731
18. Elsayed H, Stabile FM, Savio G, Bernardo E. Masked stereolithography of wollastonite-diopside glass-ceramics from novel silicone-based liquid feedstock. Open Ceram. 2023;16:100474. https://doi.org/10.1016/j.oceram.2023.100474

19. Dogrul F, Ożóg P, Michálek M, Elsayed H, Galusek D, Liverani L, et al. Polymer-derived Biosilicate®-like glass-ceramics: engineering of formulations and Additive manufacturing of three-dimensional scaffolds. Mater. (Basel). 2021;14(18):5170. https://doi.org/10.3390/ma14185170
20. Lim C-B, Yeo D-H, Shin H-S, Cho Y-S. Low temperature sintering additives for mullite ceramics. J Korean Ceram Soc. 2011;48(6):604–9. https://doi.org/10.4191/kcers.2011.48.6.604
21. Giovannelli Maizo ID, Luz AP, Pagliosa C, Pandolfelli VC. Boron sources as sintering additives for alumina-based refractory castables. Ceram Int. 2017;43(13):10207–16. https://doi.org/10.1016/j.ceramint.2017.05.047
22. Griggio F, Bernardo E, Colombo P, Messing GL. Kinetic studies of mullite synthesis from alumina nanoparticles and a preceramic polymer. J Am Ceram Soc. 2008;91(8):2529–33. https://doi.org/10.1111/j.1551-2916.2008.02515.x
23. Rau DA, Williams CB, Bortner MJ. Rheology and printability: a survey of critical relationships for direct ink write materials design. Prog Mater Sci. 2023;140:101188. https://doi.org/10.1016/j.pmatsci.2023.101188
24. del-Mazo-Barbara L, Ginebra M-P. Rheological characterisation of ceramic inks for 3D direct ink writing: a review. J Eur Ceram Soc. 2021;41(16):18–33. https://doi.org/10.1016/j.jeurceramsoc.2021.08.031
25. Ożóg P, Elsayed H, Grigolato L, Savio G, Kraxner J, Galusek D, et al. Engineering of silicone-based blends for the masked stereolithography of biosilicate/carbon composite scaffolds. J Eur Ceram Soc. 2022;42(13):6192–98. https://doi.org/10.1016/j.jeurceramsoc.2022.06.057
26. Sacks MD, Wang K, Scheiffele GW, Bozkurt N. Effect of composition on mullitization behavior of α-alumina/silica microcomposite powders. J Am Ceram Soc. 1997;80:663–72. https://doi.org/10.1111/j.1151-2916.1997.tb02882.x
27. Giovannelli Maizo ID, Luz AP, Pagliosa C, Pandolfelli VC. Boron sources as sintering additives for alumina-based refractory castables. Ceram Int. 2017;43(13):10207–16. https://doi.org/10.1016/j.ceramint.2017.05.047
28. Kracek FC, Morey GW, Merwin HE. The system water-boron oxide. Am J Sci. 1938;5:143–71.
29. Sofie SW, Dogan F. Freeze casting of aqueous alumina slurries with glycerol. J Am Ceram Soc. 2001;84(7):1459–64. https://doi.org/10.1111/j.1151-2916.2001.tb00860.x
30. Das PS. Novel-type inorganic foams from preceramic polymers with embedded titania nanoparticles for photo-catalytic applications. Adv Eng Mater. 2011;(13):996–1001. https://doi.org/10.1002/adem.201100025
31. Gibson LJ, Ashby MF. Cellular Solids: Structure and Properties. 2nd ed. Cambridge University Press;1997. https://doi.org/10.1017/CBO9781139878326
32. Zhang GJ, Yang JF, Ando M, Ohji T, Kanzaki S. Mullite–boron nitride composite with high strength and low elasticity. J Am Ceram Soc. 2004;87:296–98. https://doi.org/10.1111/j.1551-2916.2004.00296.x

How to cite this article: Diamanti V, Elsayed H, Bernardo E. 3D-printed porous mullite lattice structures by hybrid direct ink writing of silicone suspension-emulsions. J Am Ceram Soc. 2025;108:e20290. https://doi.org/10.1111/jace.20290